J. Ocean Univ. China (Oceanic and Coastal Sea Research)
https://doi.org/10.1007/s11802-019-3860-3
ISSN 1672-5182, 2019 18 (4): 868-882
http://www.ouc.edu.cn/xbywb/
E-mail:xbywb@ouc.edu.cn

Morphodynamics of an Artificial Cobble Beach in Tianquan Bay, Xiamen, China

SHU Fangfang[1), 2)], CAI Feng[2), *], QI Hongshuai[2)], LIU Jianhui[3)], LEI Gang[2)], and ZHENG Jixiang[2)]

1) *College of Marine Geosciences*, *Ocean University of China*, *Qingdao* 266100, *China*
2) *Third Institute of Oceanography*, *Ministry of Natural Resources*, *Xiamen* 361005, *China*
3) *Island Research Center*, *Ministry of Natural Resources*, *Pingtan* 350400, *China*

(Received March 29, 2018; revised May 7, 2018; accepted May 22, 2018)
© Ocean University of China, Science Press and Springer-Verlag GmbH Germany 2019

Abstract By tracking and monitoring the profile configuration, topography, and hydrodynamic factors of an artificial cobble beach in Tianquan Bay, Xiamen, China over three consecutive years after its completion, we analyzed the evolution of its profile configuration and plane morphology, and its storm response characteristics. The evolution of the profile configuration of the artificial cobble beach in Tianquan Bay can be divided into four stages. The beach was unstable during the initial stage after the beach nourishment the profile configuration changed obviously, and an upper concave composite cobble beach formed gradually, which was characterized by a steep upper part and a gentle lower part. In the second stage, the cobble beach approached dynamic equilibrium with minor changes in the profile configuration. At the third stage the beach was in a high-energy state under the influence of Typhoon Meranti, and the response of the artificial cobble beach differed significantly from that of the low-tide terrace sandy beach. Within a short time, there was net onshore transport of cobbles in the cross-shore direction. The beach face was eroded, the beach berm was accumulated, and the slope of the beach was steepened considerably. In the alongshore direction, there was notable transport of cobbles on the beach from east to west along the shore, and the total volume of the beach decreased by 4.5×10^3 m^3, which accounted for 50% of the total amount of beach volume lost within three years. The fourth stage was the restoration stage after the typhoon, characterized by a little gentler profile slope and the increase in width and the decrease in height of beach berm. Because of the action of waves and the wave-driven longshore current caused by the specific terrain and landform conditions along the coast (*e.g.*, coastal headlands, near-shore artificial structures, and reefs), the coastline of the artificial cobble beach gradually evolved from being essentially parallel to the artificial coast upon completion to a slightly curved parabolic shape, and three distinct erosion hotspots were formed on the west side of the cape and the artificial drainpipe, and the reefs. Generally, the adoption of cobbles for beach nourishment on this macro-tidal coast beach with severe erosion has yielded excellent stability and adaptability.

Key words beach nourishment; cobble beach; morphologic evolution; erosion hotspot; storm response

1 Introduction

Because of the influence of a series of natural processes and anthropogenic activities (such as global climate change, increases in sea level, and continuous increases in exploitation and degree of utilization of coastal zones), coastal erosion has become one of the main threats to the ecological environment in coastal zones and restricts the development of marine economies (Bruun, 1988; Cai *et al.*, 2009; Van Rijn, 2011; Pilkey Jr. and Cooper, 2014; Neumann *et al.*, 2015). Approximately 70% of sandy coastlines around the world are in a state of erosion and retreat (Bird, 1985), and that proportion is still growing. Therefore, various approaches to coastal protection have been adopted. In particular, beach nourishment, as one widely applied means of ecological 'soft engineering', has become a preferred option to relieve the erosion of sandy coasts and to protect coastlines (Gorzelany and Nelson, 1987; Dixon and Pilkey Jr., 1991; Davison *et al*., 1992; Hanson *et al*., 2002; Dean, 2005; Cai *et al*., 2011; Aragonés *et al*., 2015).

For coastal segments with strong erosion, the beach nourishment method employing sandy sediments is often used but has the shortcoming of poor stability, short engineering lifetimes, and high costs (Pilkey, 1990), and storm surges and typhoon waves can generate devastating effects (Anthony, 2005; Haerens *et al*., 2012; Castelle *et al*., 2015; Masselink *et al*., 2016). Because gravel (cobble) beaches are characterized by coarser sediment, high permeability, and high porosity, they have stronger energy dissipation effects and better stability than sandy beaches (Austin and Masselink, 2005; Osborne, 2005; Pedrozo-Acuña *et al*., 2008). Therefore, the adoption of coarse-grained sediments like gravel or cobbles for beach nourishment on coasts with strong erosion and high energy is

* Corresponding authors. Tel: 0086-592-2195282
E-mail: fcai800@126.com

an effective approach to relieve erosion of sandy beaches (Kirk, 1992; Aminti *et al*., 2003; Cammelli *et al*., 2006; Bergillos *et al*., 2017).

A gravel beach is not prone to movement under the conventional dynamic action but generally moves under storm conditions, and is therefore conducive to resisting erosion caused by storms on coasts (Alegria-Arzaburu and Masselink, 2010; Chen *et al*., 2011; Stark and Hay, 2016). The main characteristics of profile variation in the surf zone of a gravel beach are the strong trend of transportation toward the shore and the formation of a gravel beach berm. The weaker strength of backwash flows compared with uprush currents, caused by infiltration loss, is usually the reason that gravel beaches are steeper than sandy beaches, and the impacts of plunging waves generated by steep slopes and wave force play important roles in the morphological evolution of gravel beaches (Austin and Masselink, 2006; Pedrozo-Acuña *et al*., 2007).

The first artificial gravel beach was built on the Georgian coast of the Black Sea, where hard-defences had failed to protect against coastal erosion (Zenkovich and Schwartz, 1987). After that, the United States, New Zealand, Italy, and Spain also carried out gravel beach nourishment on some coasts with strong erosion (Lorang, 1991; Aminti *et al*., 2003; Cammelli *et al*., 2006; Bergillos *et al*., 2015).

Although gravel beach nourishement have been applied more than 30 years, few morphodynamic studies have been performed on artificial coarse-grained beaches. By surveying three artificial pebble beaches located at Marina di Pisa, Bertoni and Sarti (2011) found that both longshore and cross-shore transports were capable of moving coarse-grained sediments and the beach berm showed a remarkable retreat during storms. Bergillos *et al*. (2016) suggested that mixed sand and gravel beaches could recover faster from storm erosion than sandy beaches, and the long-term benefit of the artificial nourishment was influenced by the sediment grain size used for the nourishment and its placement on the beach. Grottoli *et al*. (2017) highlighted that storms tended to accumulate materials towards the upper part of the beach with no shoreline rotation and no chance to recover the initial configuration.

Observations and studies on the long-term dynamic morphologic evolution of artificial gravel beaches, especially the response, adjustment, and recovery processes of profiles under extreme hydrodynamic conditions, are relatively insufficient compared with those of sandy beaches. In this paper, based on topographic monitoring and periodic profile measuring over three consecutive years after completion of the first artificial cobble beach in Tianquan Bay, Xiamen, China, and based on observations of local meteorological and hydrodynamic conditions, especially the effects of Typhoon Meranti, we studied the evolutionary characteristics of profile configuration and plane morphology during different time periods after nourishment of the artificial cobble beach. The generation mechanism of the erosion hotspot and the response characteristics of this beach to the storm were attempted to be investigated.

2 Background

2.1 Study Area Setting

The Tianquan Bay (Fig.1) is located along the southern coast of Xiamen Island on the western shore of the Taiwan Strait and the coast exhibits an east-west trend. It begins in the west at the Zengcuoan cape and extends eastward until the pedestrian bridge of Baishi cape. The length of this segment of the coastline is approximately 1.0 km. A staircase revetment was constructed along the coast, and the natural sediments on the beach are fine- to medium-grained sand. Because of the influence of prevailing wave scouring from open seas and the insufficient sediment supply caused by the turning of the coastal current, this coastal segment has some of the severest erosion in southeastern Xiamen Island. Shore protection structures and the wooden trestle road have been destroyed several times during typhoon storm surges, and bedrock gravel is exposed on the beach (Fig.1d). To protect the coast and mitigate the severe erosion, the first artificial cobble beach (Fig.1c) in China was built on the coast of Tianquan Bay in June 2014. The length of the coastal line on the artificial cobble beach is 632 m, and the designed slope of the profile is 1:5. The 5–10 cm cobblestones were paved. The designed elevation of the 479-m-long beach berm on the west side is 4.0 m (the datum line refers to the National Vertical Datum 1985 hereinafter), and the designed elevation of the 153-m-long beach berm on the east side is 3.0 m.

The research area falls within the regular semi-diurnal tidal area; the multi-year mean spring high-tidal level is 3.81 m, the multi-year average tidal range is 3.98 m, and the maximum tidal range of historical years is 6.92 m (Liao *et al*., 2010; Fu *et al*., 2013). It is a macro-tidal coast. The annual average wind velocity on the coast of Tianquan Bay is 3.3 m s^{-1}, and the prevailing wind direction is southeast, with the occurrence frequency of 11.16%. The maximum wind velocity in separated directions is 26.7 m s^{-1} in the north direction. The annual average significant wave height observed by the 'AWAC' wave-measuring buoy (Fig.1b) at 10-m water depth, 1.5 km away from the shore is 0.33 m. The mean wave period is 3.0 s, and the annual average spectral peak period is 6.0 s. The prevailing wave direction is south-southeast, with a frequency of occurrence of 43.91%. The annual average and annual maximum wave heights (Hs) in this direction are 0.32 m and 0.91 m, respectively. Rose charts of winds and waves are shown in Fig.2.

2.2 Typhoon Meranti

Typhoon Meranti (201614, Fig.1a) was generated at 14:00 (Beijing time hereinafter) on September 10 in the western Pacific Ocean and then moved northwest. At night on September 13, the maximum wind velocity in the vicinity of the storm's center reached 70.0 m s^{-1}, and the lowest pressure at the center was 900 hPa. At 10:00 on September 14, it swept the southern end of Taiwan Island

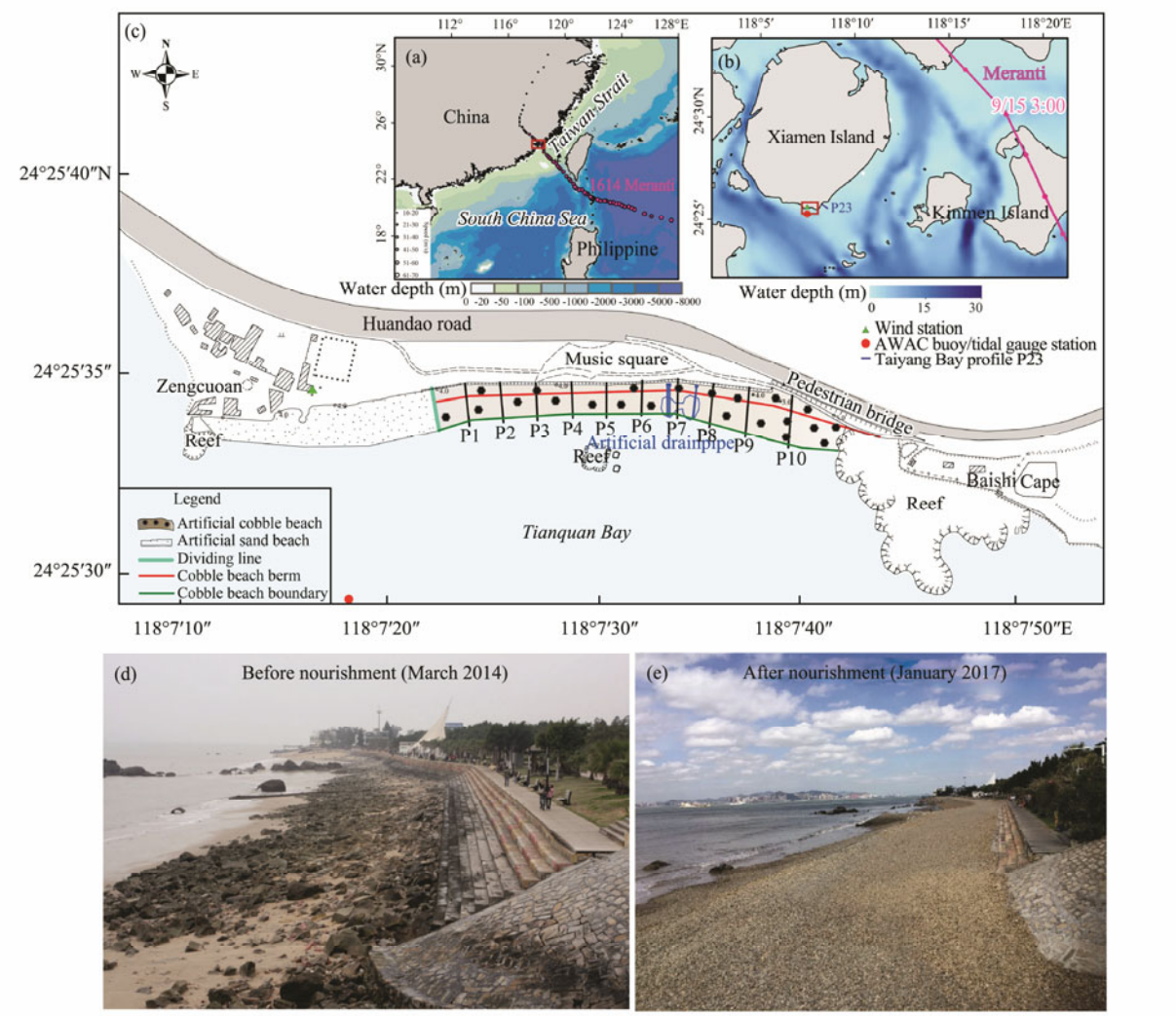

Fig.1 The location of the research area and photos of beach. a, path of typhoon Meranti; b, location of the observation station; c, topographic map of the artificial cobble beach; d, photo before nourishment; e, photo after nourishment.

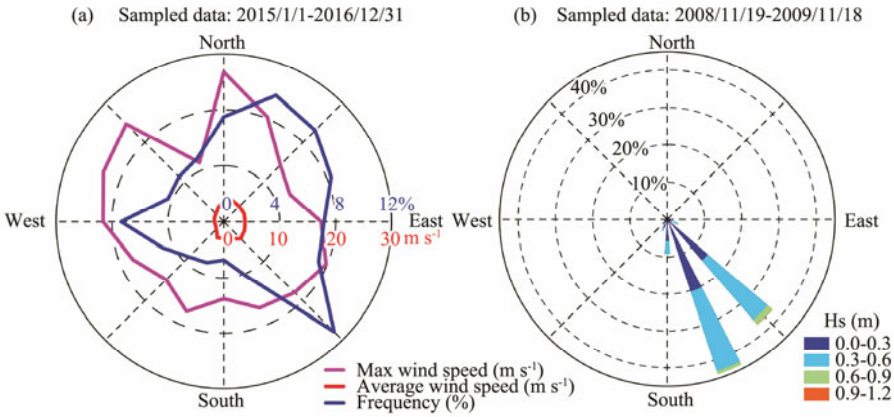

Fig.2 Rose charts of winds and waves in the research area. a, 10-min average wind velocity for 2015–2016; b, Hs wave rose chart for 2009.

and entered the Taiwan Strait, and at 3:00 on September 15, it landed as a strong typhoon in Xiamen City, Fujian Province, China. The central pressure upon landing was 945 hPa, and the central maximum wind velocity was 52.0 $m\,s^{-1}$. The landing site was approximately 20 km northeast of the artificial cobble beach of Tianquan Bay (Fig.1b). The maximum ten-minute wind speed measured in Tianquan Bay was 33.1 $m\,s^{-1}$, and the instantaneous maximum wind velocity reached 49.0 $m\,s^{-1}$. Upon the landing of the typhoon, the wind direction in the research area was due

north, and the observed tide level was −0.20 m, in the low-tide period of an ebb tide.

After the typhoon landed, the wind direction was deflected from north to northwest and southwest, and the maximum storm surge and typhoon wave height both occurred at 5:00. The maximum storm surge value reached 0.95 m, and the maximum wave height (Hs) was 2.69 m (Fig.3). Meranti weakened to a tropical depression at 17:00 on that day, and dissipated in the Yellow Sea area of China on the morning of September 16.

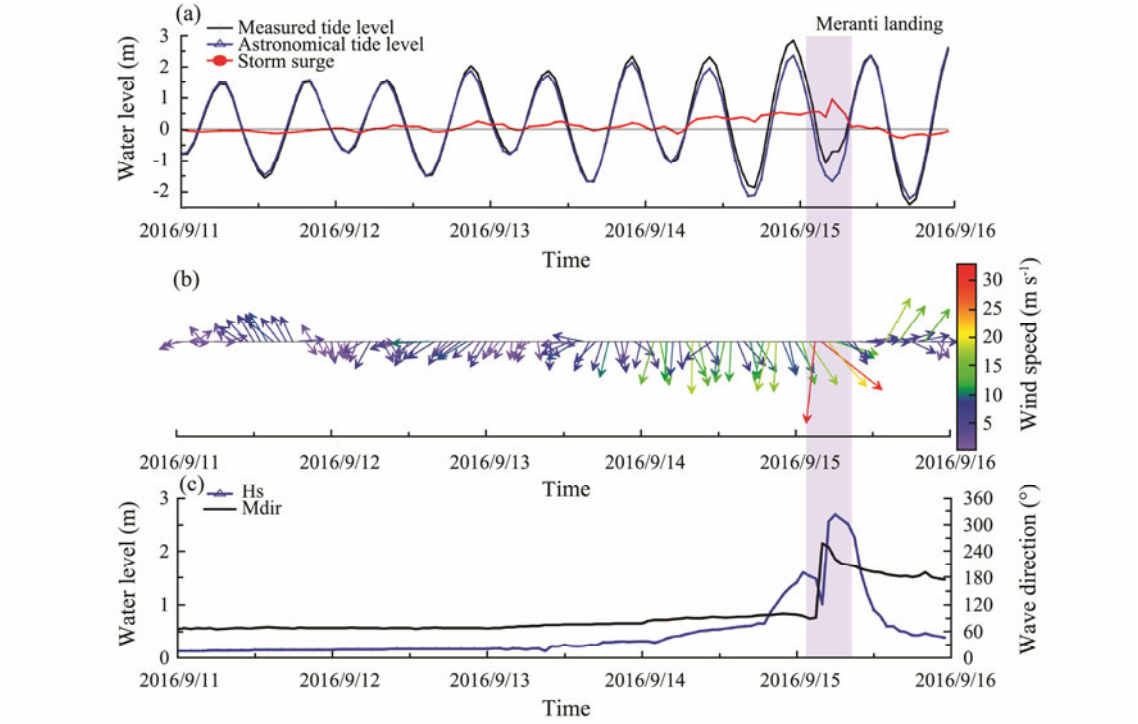

Fig.3 Changing curves of tide level, wind speed, and wave height in the research area during Typhoon Meranti. a, tidal level; b, wind speed; c, wave height.

3 Methods

3.1 Profile Measurements and Analysis

We employed ten typical profiles, P1–P10, for the measurements (Fig.1c) and the interval between any two adjacent profiles was approximately 50 m. According to the direction of each profile, we employed a Trimble RTK-GPS to repetitively measure the profile configuration of the beach. The horizontal error in measurement accuracy was smaller than 1 cm, and the vertical error was smaller than 2 cm.

After the completion of the cobble beach, from June 2014 to May 2017, we conducted profile measurements on the beach 10 times, in June 2014, March, August, and October 2015, January, May, and September 2016 (twice, before and after 201614 Typhoon Meranti), and January and May 2017 respectively. We analyzed the profile measurement data, and the specific elements are shown in Fig.4.

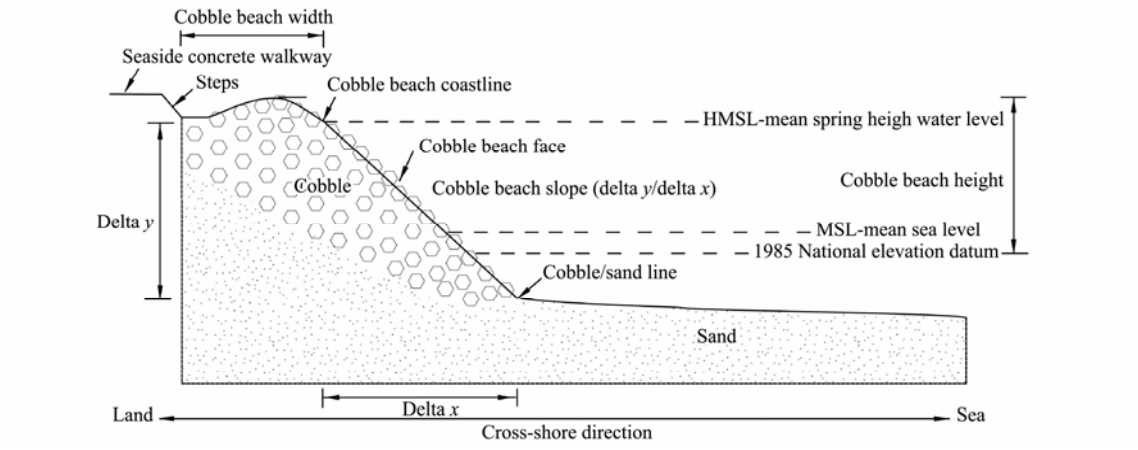

Fig.4 Definition sketch of the cobble beach in Tianquan Bay.

3.2 Beach Topographic Data

In June 2014, July 2016, and January 2017, we employed the Trimble RTK-GPS to measure the topography of the cobble beach, and the measurement accuracy was the same as the accuracy of the profile measurements. The horizontal error was smaller than 1 cm, and the vertical error was smaller than 2 cm. The measurement results were corrected by using control points.

3.3 Orthophoto Images

In October 2017, we employed a Switzerland SenseFLY-eBee (RTK) unmanned aerial vehicle (UAV) aerial survey system to conduct photographic measurements of the artificial cobble beach in Tianquan Bay. The system was used with the RTK GNSS function and high-precision digital orthophoto images of the research area were obtained.

3.4 Numerical Simulation of the Wave Field and the Wave-Induced Current

For the numerical simulation of the wave field and the wave-induced current on the artificial cobble beach, the FUNWAVE-TVD model was adopted. The FUNWAVE model is the fully nonlinear Boussinesq wave model initially developed by Kirby *et al*. (1998) from the University of Delaware. FUNWAVE-TVD, developed by Shi *et al*. (2012, 2013), is the latest version of the FUNWAVE model. It solves Boussinesq equations with the shock-capturing TVD scheme. It is versatile in modeling wave refraction, diffraction, reflection, and deformation effects and can be used to simulate three-wave interaction of waves, water flows, and shallow-water long waves and the interactions between waves and structures. It has been successfully validated against a series of coastal engineering applications (Ha *et al*., 2014; Su *et al*., 2015). In this paper, we use FUNWAVE-TVD to simulate the wave field and the wave-driven flow field on the artificial cobble beach. The numerical model is forced with annual mean tidal level and maximum significant wave height in the SSE direction along the offshore boundary. We deflected the terrain of the cobble beach anti-clockwise by 5° and adopted a relative coordinate system. The real bathymetry is mapped to 200×500 grid, with a uniform grid resolution of 2 m. The bathymetric terrain was determined by the measurement results of a Hi-Target HD-27T echo digital sounder and RTK, the incident boundary wave condition was determined by the statistical value of the observation results for the 'AWAC' wave-measuring buoy, and the statistical values of the regional wind field condition were measured by using R. M. YOUNG sensors.

4 Results

4.1 Changes in the Profile Configuration of the Artificial Cobble Beach

The profile configurations during different periods for P1–P10 are shown in Fig.5. Upon completion, the profile of the cobble beach exhibited a straight steep slope with the slope of 1:5. From the initial completion to March 2015, there was an obvious change in the profile configuration, and the coastline of the cobble beach and the cobble/sand line retreated toward the land side. The beach berm rose to form the berm crest, which results in an upper concave profile configuration. According to the five monitoring results from March 2015 to September 2016 (before Typhoon Meranti), the changes of configurations in most profiles were very small. During Typhoon Meranti, the beach face was eroded, the cobbles were transported toward the shore, the height of the beach berm increased, the slope of the profile steepened, and the upper concave amplitude increased. After the typhoon, the height of the beach berm decreased, and the profile became a little gentler.

4.1.1 Beach berm

We define the height of the beach berm as the height at the highest point in the beach profile. The coastline of the cobble beach is the inter one of the multi-year mean spring high-tidal level and the profile of the cobble beach, and the width of the beach berm is the distance from the beginning point on the land side to the coastline of the cobble beach.

Within three years after the completion of the cobble beach, the height of the beach berm (Fig.6a) generally exhibited increase, with an average of 0.50 m. In particular, the designed elevation of beach berm in P10 was lower than those in the other profiles, and the height increased by 1.40 m. Among the other profiles, the heights in P5, P6, and P9 increased by 0.56, 0.53, and 0.45 m, respectively. The increments in height for the beach berm in P1, P2, P3, and P8 were smaller than 0.25 m. According to the results of 10 repeated observations, the largest variation in the height of the beach berm within three years occurred in the initial stage, from the time of completion to March 2015, and the average increase in height was 0.46 m. this increase was followed by the period of time during which Typhoon Meranti occurred, when the height of the beach berm increased by 0.30 m on average within a short time.

Within three years after completion, the width of the beach berm on the cobble beach generally reduced (Fig.6b), and the average reduction was 4.65 m. There was a relatively large difference for the variation ranges of the beach berm widths in different profiles. In particular, in P10 beach berm narrowed from 20.00 m to 8.98 m, with retreat of 11.02 m. In P6 it narrowed from 15.00 m to 5.30 m, with the erosion and retreat of 9.70 m. In P9 the beach berm narrowed from 19.00 m to 18.30 m, with erosion and retreat of 0.70 m. And in P8 it widened from 18.00 m to 19.30 m, with an increase of 1.30 m. Within three years, the degree of erosion and retreat, in terms of the width of the beach berm, was greatest from the initial stage of completion to March 2015, when the average erosion was 3.68 m. During Typhoon Meranti, the average erosion evaluated by the width of the beach berm was 0.96 m.

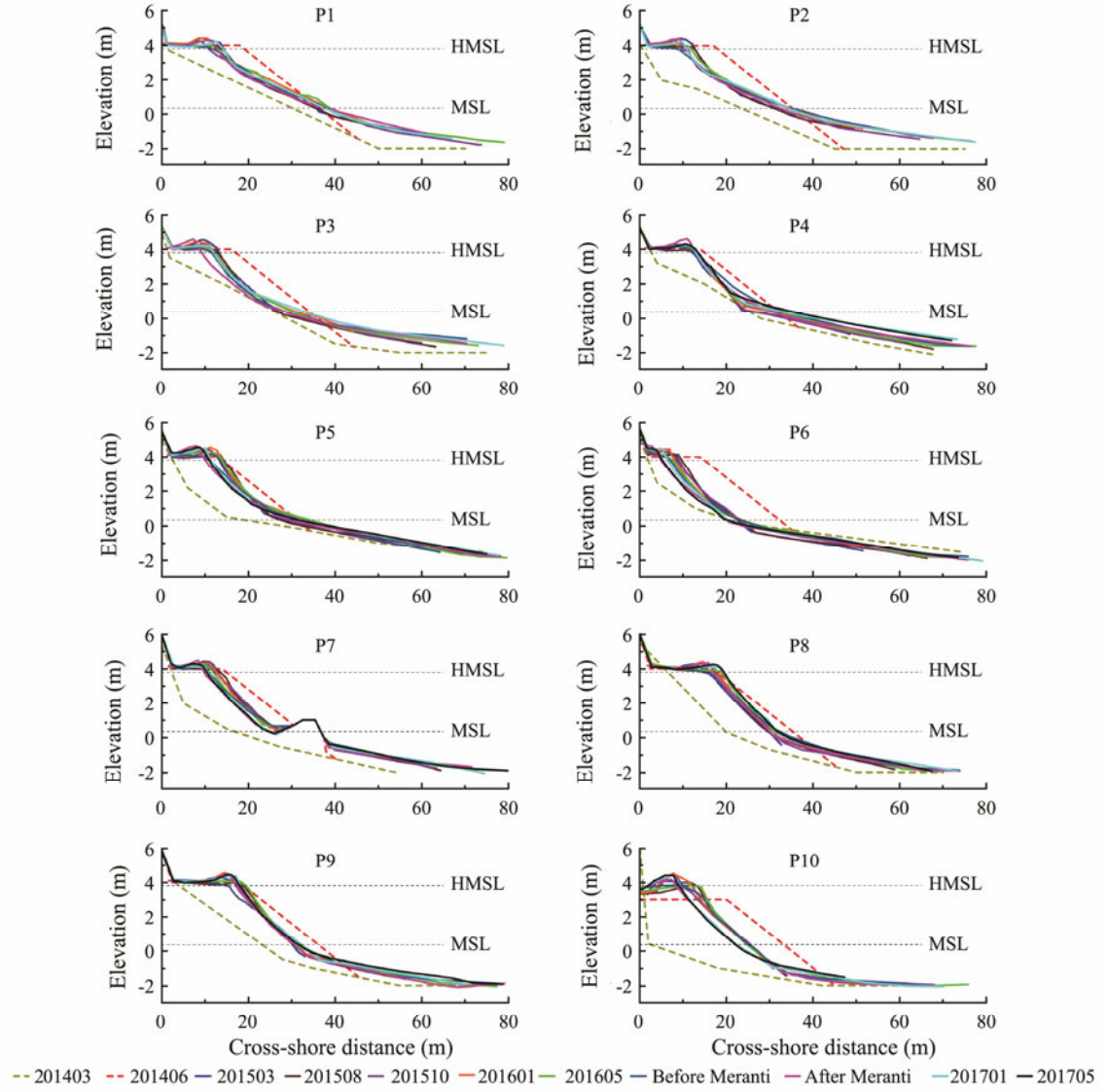

Fig.5 Variations in the profile configuration of the artificial cobble beach in Tianquan Bay.

4.1.2 Intertidal beach slope

The cobble/sand line is defined as the boundary line where the surface sediments transform from cobbles to sand, and the slope of the cobble beach is the slope value between the coastline of the cobble beach and the cobble/sand line. The slopes of the profile P1–P10 at the different periods are shown in Fig.6c. Upon completion, the slope of the profile was 1:5, and within three years of completion, the profile of the cobble beach had generally been steepening. The average slope increased by 0.04. In particular, the increases for profile P4–P8 were largest. The average slope increased by 0.11, 0.08, 0.06, 0.07, and 0.08 for these profiles, respectively. The slope for P9 increased by 0.04, and the slopes for P3 and P10 both increased by 0.01. The westernmost profiles, P1 and P2, became slightly gentler, with the average slope decreasing by 0.06 and 0.01, respectively. Based on the 10 sets of observational results, all ten typical profiles steepened after Typhoon Meranti, and the average slope increased by 0.05.

4.1.3 Variation of sediment volume

When we statistically analyzed the volume per unit width of the profiles, we set the farthest transverse distance from the shore was to the location of the cobble/sand line upon completion. The total quantity of cobblestones used in the artificial cobble beach of Tianquan Bay was approximately $40.9\times10^3\,m^3$. Within three years after completion, the average volume per unit width along the profile decreased by $14.4\,m^3\,m^{-1}$. The variations in the volume per unit width for each profile at different times are shown in Fig.7, and the reduction in total volume was approximately $9.1\times10^3\,m^3$, which accounted for 22% of the input quantity. From the initial completion to March 2015, the variation of the profile was relatively violent, and the average volume per unit width decreased by $17.8\,m^3\,m^{-1}$. From March 2015 to September 2016 (prior to the typhoon), the average volume per unit width increased by $5.2\,m^3\,m^{-1}$. After Typhoon Meranti, the average volume

per unit width decreased by 7.2 $m^3 m^{-1}$; from then to May 2017, the average volume per unit width of the cobble beach increased by 5.5 $m^3 m^{-1}$. We could find that the initial stage of nourishment was the most unstable.

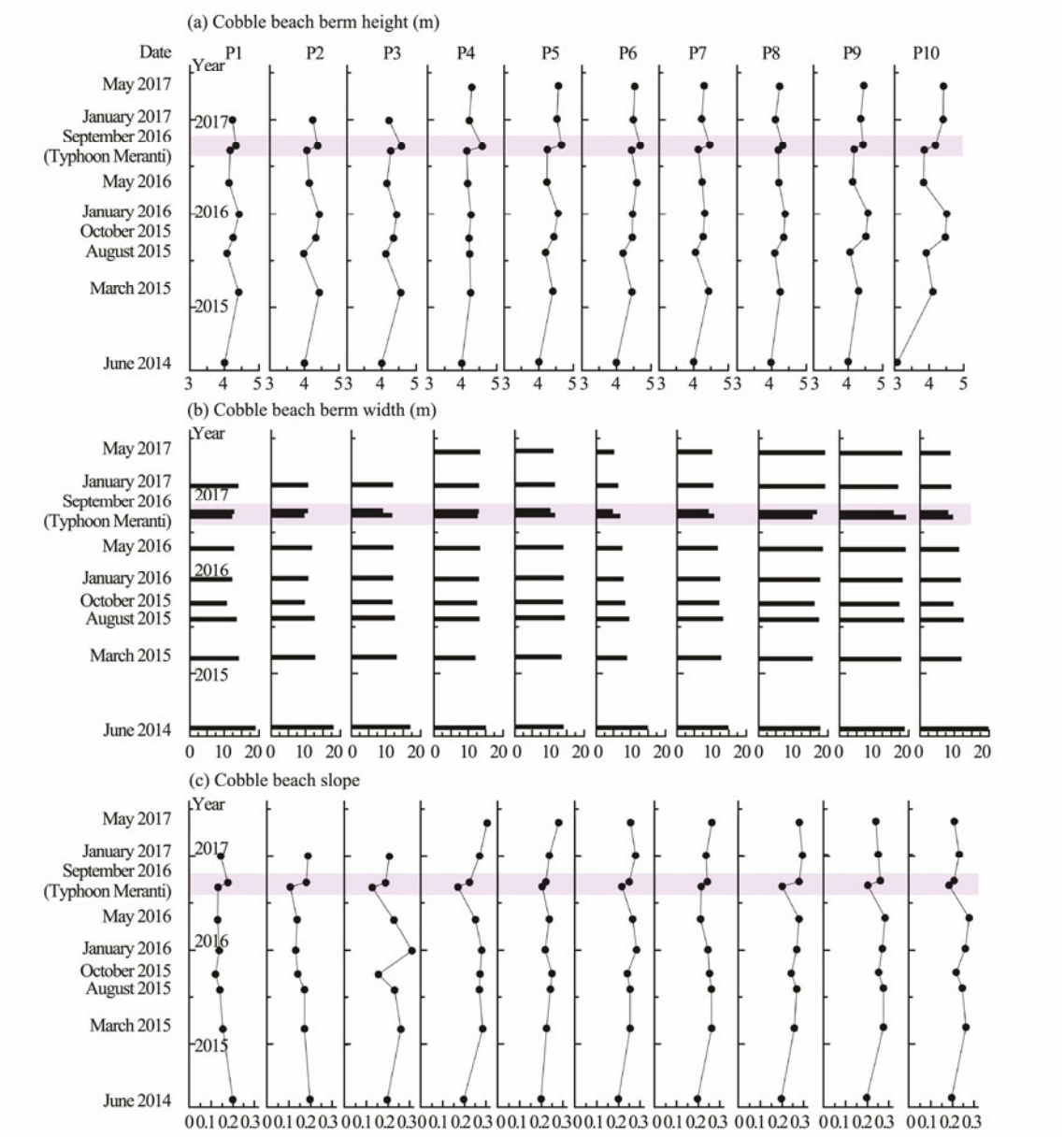

Fig.6 Variations in the height and width of the beach berm and the profile slope for the representative profiles in Tianquan Bay.

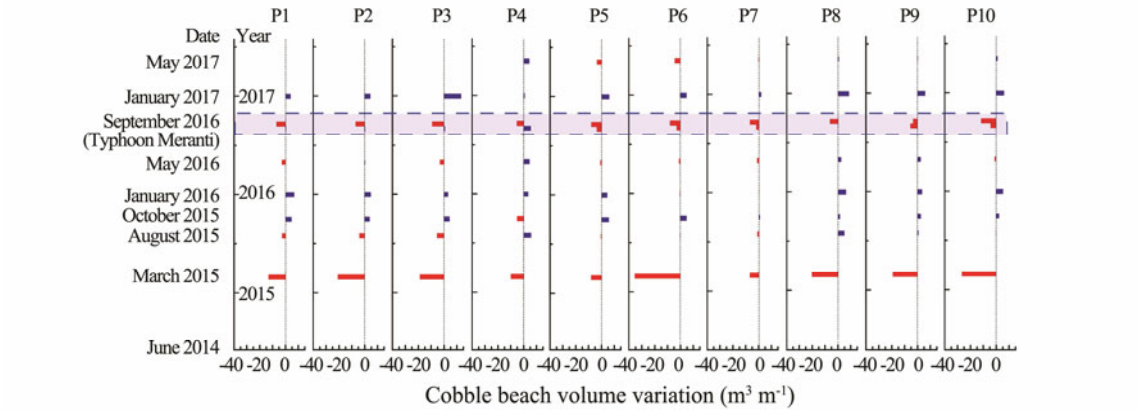

Fig.7 Variations in the volume per unit width of each profile. Red color, decrease; blue color, increase.

4.2 Variation in the Plane Morphology of the Artificial Cobble Beach

The variations in the artificial cobble beach coastline and the morphology of dispersed cobble belt during different periods are shown in Fig.8.

Coastline of the cobble beach: In March 2015, there was a certain degree of coastline retreat in different regions of the cobble beach relative to that upon completion. In particular, the retreat on the west side near the cape rock of Baishi and the artificial drainpipe rock was relatively obvious, and the maximum retreat was close to 8.0 m. There was also a retreat of 4.0–5.0 m for the westernmost coastline of the cobble beach. In July 2016, there was a small degree of advance toward the sea for the coastline on the east side, and the maximum advance was close to 1.5 m. The coastline to the west of the middle drainpipe rock and that on the westernmost of the cobble beach retreated slightly. In May 2017, the coastline to the west of Baishi cape and the drainpipe rock continued to retreat (approximately 3.0–5.0 m), forming two arc coastlines with rocks as the cape head. The degree of retreat in the other regions was smaller than in these two regions, whereas the coastline on the west side of the cobble beach exhibited the seaward advance of 1.0–3.0 m.

Dispersed cobbles belt: In July 2016, a distinct wedge-shaped diffusion zone had formed to the west of the cobble beach. The region was approximately 250 m long, and the average width was approximately 20 m. Some of the cobbles were scattered on the upper level of the sandy beach, and some were present on the lower level of the sandy beach, forming the sand-gravel mixed layer. The monitoring results in May 2017 revealed that the diffusion zone continued to extend westward approximately 26 m compared with that in July 2016, and the width of the belt on the side near the cobble beach became slightly narrower. The maximum width of narrowing was approximately 10 m. The on-site survey found that although the surface layer at the narrowing place was composed of sandy materials, it had cobbles buried underneath.

4.3 Erosion Hotspots

From the perspective of coastline variation for the cobble beach from its completion to May 2017 (Fig.9b), there was stronger erosion and retreat in the eastern, middle, and western profiles than in adjacent regions, and the greatest amounts of coastline retreat in the eastern, middle, and western profiles reached 17.00, 9.50, and 5.80 m, respectively. In July 2016, in comparison with the terrain upon completion (Fig.9c), there was obvious erosion on the beach face to the west of the Baishi cape, to the west of the drainpipe rock and in the west of the cobble beach, among which the maximum erosion approached 2.50 m. There was relatively obvious accumulation at the bottom corner of the western beach face and the eastern beach berm. In particular, the maximum accumulation at the bottom corner of the western beach face exceeded 1.00 m. In January 2017, in comparison with the terrain upon completion (Fig.9d), the erosion in the middle of the beach face had further expanded, and the maximum erosion in the middle of the beach face to the west of the drainpipe rock reached 3.00 m. The beach berm and its upper part were primarily under the state of accretion, and the maximum accretion at the beach berm near the Baishi cape on the east side was close to 1.50 m. Based on the orthophoto image (Fig.9a), there were three distinct regions of erosion hotspots present in the cobble beach. From east to west, they were on the west side of the Baishi cape (A), the west side of the artificial drainpipe rock (B), and the west side of the lower reach of the natural reefs (C). The degrees of erosion at the sites A and B were stronger than that at site C.

4.4 Response of the Artificial Cobble Beach to Typhoon Meranti

Before and after Typhoon Meranti, the variation in the profile configuration of the artificial cobble beach (Fig.10) was relatively significant, and it generally exhibited the net transportation of cobbles onshore in the cross-shore direction. The beach face was eroded, and the cobbles accumulated in the upper part of the beach berm, forming the obvious bump on the beach berm. The height of the beach berm increased by 0.30 m on average. In particular, the height of the beach berm increased to 4.69 m in P6, which was the highest in the region. The slope of the profile generally became steeper, and the average slope increased by 0.05. In particular, the steepest slope reached 0.28 in P8, and the gentlest slope was 0.18 in P2, whose slope also increased by 0.07 after the typhoon. The variation characteristics of the width of the beach berm differed

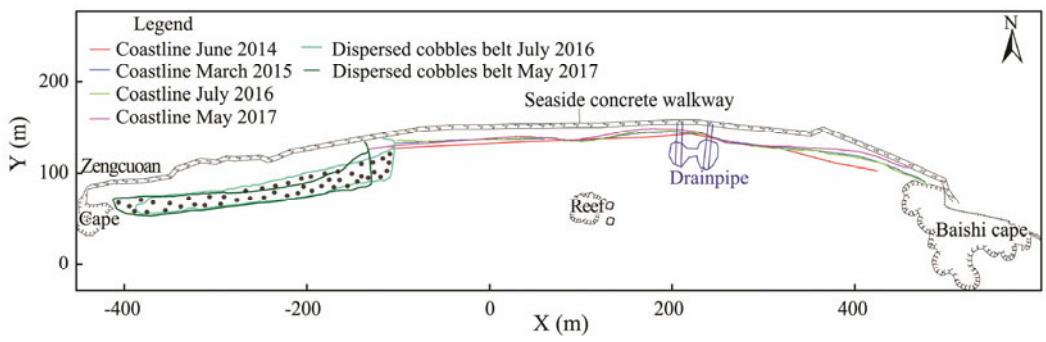

Fig.8 Variation in the coastline of the artificial cobble beach and the morphology of dispersed cobble belt.

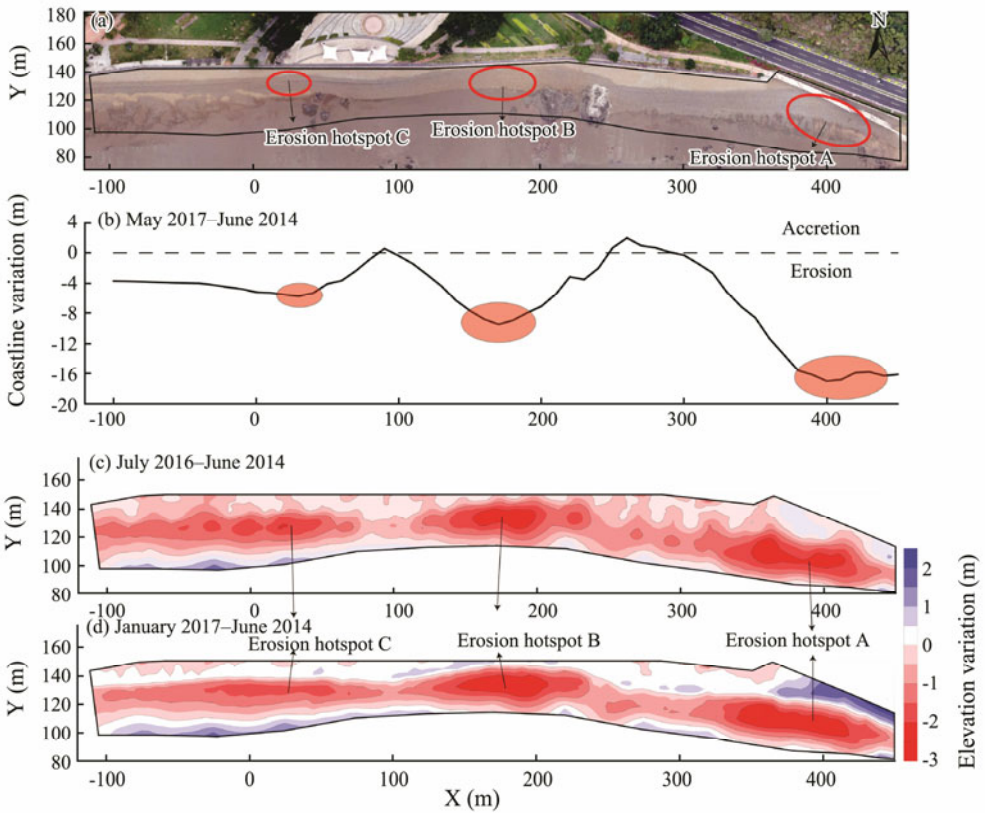

Fig.9 Topographic variations of the cobble beach and the erosion hotspots. a, locations of erosion hotspots marked on the orthophoto image taken in October 2017; b, variation of coastline, between May 2017 and completion; c, variation in terrain, between July 2016 and completion; d, variation of terrain, between January 2017 and completion.

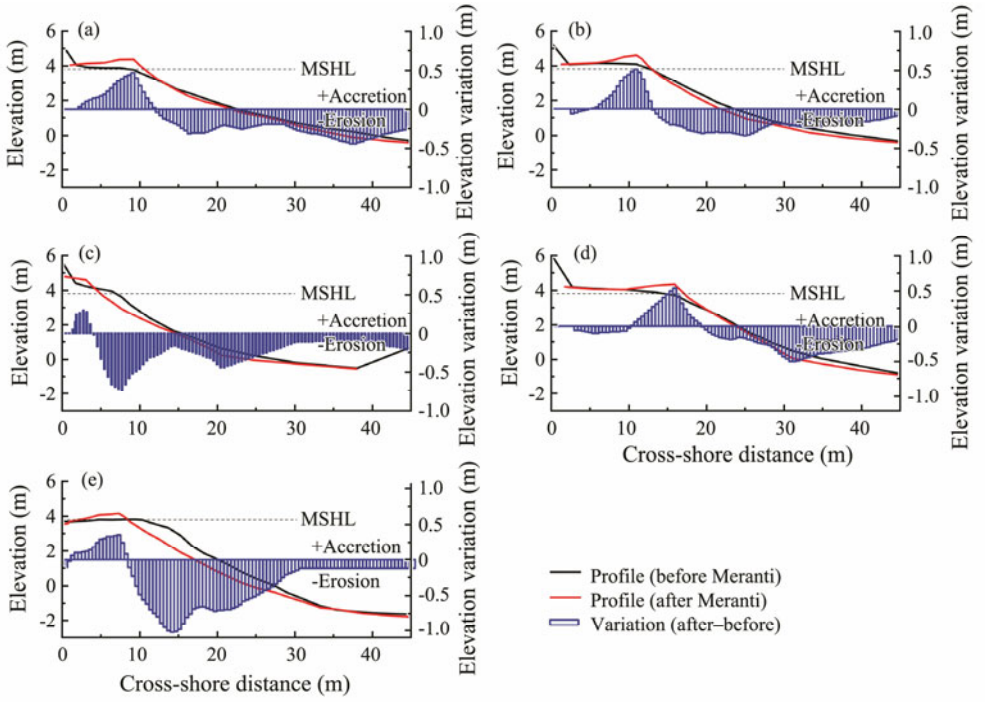

Fig.10 Variations of representative profiles before and after Typhoon Meranti. a, profile P2; b, P4; c, P6; d, P8; e, P10.

according to the location of the profile. The widths of the beach berms narrowed considerably in P6 and P10, with erosion of 2.15 m and 1.37 m, respectively. The accretion width on profiles P2 and P8 exceeded 1.00 m, and the width of the beach berm in P4 remained essentially unchanged.

In the alongshore direction, the cobble beach experienced obvious transport from east to west. In particular, at the beach face 10.00–20.00 m from the shore, P10 was severely eroded, whereas P8 was accreted. On the beach

face about 5.00–10.00 m from the shore, the erosion in P6 was severe, whereas P4 and P2 on the west side of beach underwent accretion. Fig.10 shows the variation in the elevations of different profiles, and the maximum heights of accumulation for the representative profiles (P2, P4, P6, P8, and P10) from east to west were 0.35, 0.54, 0.30, 0.51, and 0.47 m, respectively, located 7.30, 15.90, 2.70, 10.90, and 9.10 m from the shore, respectively. Erosion on the profile of the cobble beach was severest for P10 and P6. In particular, the severest erosion locates 14.10 m from the shore along P10, where downward erosion exceeded 1.00 m. The maximum erosion on the beach face in P6 was 0.74 m, which occurred 7.70 m from the shore. The maximum erosion along profiles P2, P4, and P8 did not exceed 0.50 m. Using a profile volume method, we calculated that after the typhoon, the average volume per unit width of the profile decreased by 7.2 $m^3 m^{-1}$, and the total volume lost from the cobble beach was about 4.5×10^3 m^3, which accounted for 11% of the restoration amount added on the cobble beach. The loss due to one typhoon event accounted for 50% of the total amount lost on the beach.

5 Discussion

5.1 Evolution of Profile Configuration

The profile configuration of the beach is the product of the interactions between the dynamic factors of waves, tidal currents, and winds, as well as the terrain and topography of the beach (Hine, 1979; Austin and Masselink, 2006). Under the actions of energetic tides and waves, the cobbles are constantly corroded and transported (Chen and Stephenson, 2015). Because the positive correlation of the slope of the cobble beach with the size of the cobbles, the action of waves on the cobble beach differs significantly from on the sandy beach. When a wave acts on the cobble beach, the uprush causes the cobbles to roll and move upward. The porosity of the cobble beach is significantly larger than that of the sandy beach, so the infiltration velocity is much greater than that of the sandy beach when the backwash acts. Because of the factors of infiltration and frictional resistance, the backwash intensity on the cobble beach declines substantially, and the backwash is weaker than the uprush. Therefore, it is difficult to bring all the cobbles from the beach berm back to the beach face. The difference between uprush and backwash results in the net transportation toward the shore in the swash zone, and accumulated cobbles form the beach ridge on the beach berm, and results in the steepening of profiles (Austin and Masselink, 2005; Austin and Buscombe, 2008). Data from previous researches after the completion of an artificial cobble beach were mostly obtained within three months to one year (Pye and Blott, 2009), and there is lack of long-term continuous observation data. In this study, based on 10 times profile-configuration monitoring over three years, we were able to divide the evolution of the profile configuration of the artificial cobble beach into four stages (Fig.11).

The first stage was the initial unstable stage after the beach nourishment, during which there was an obvious change in the profile configuration. The coastline of the cobble beach and the cobble/sand line receded toward the land side, and the beach berm rose to form the berm crest, forming an obvious upper concave composite cobble beach that was steeper in the upper part and gentler in the lower part. The slopes in the upper part of a cobble beach and the lower part of a sandy beach are notably different, and the slope break point is apparent (López *et al*., 2015). Generally, the erosion rate at the initial stage after nourishment was considerably higher than that at later the high-energy events (Bertoni and Sarti, 2011).

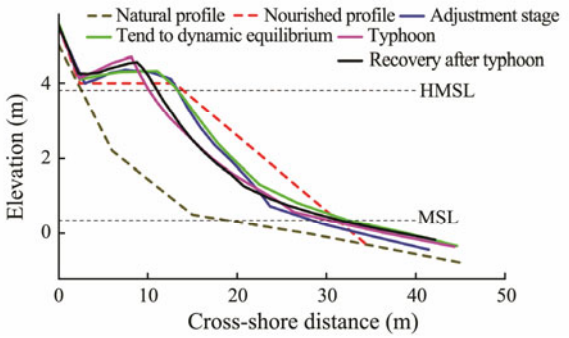

Fig.11 Evolution model of the typical profile configuration for the artificial cobble beach.

At the second stage the beach approached dynamic equilibrium. Under the action of local conventional dynamic conditions, the artificial cobble beach gradually approached an equilibrium state, and the change in profile configuration was very small. The width and height of the beach berm and the slope of the profile changed slightly in an observation season. The slope of the cobble beach typically steepened, and the beach berm typically became higher because of the accretion in autumn and winter, whereas the slope became gentler, and the height of beach berm declined in spring and summer. The variation characteristics are relatively consistent with the seasonal variation of typical tidal levels and waves in the sea area of Xiamen. The tidal level in the sea area of Xiamen is lower in spring and summer and higher in autumn and winter. It is generally lowest in April–July and highest in September–November (Liao *et al*., 2010; Fu *et al*., 2013). Without the influence of typhoons, wave energy strength is lower in spring and summer and higher in autumn and winter. It is prone to the influence of typhoons in autumn and affected by waves and storm surges with higher energies than the normal state. The third stage was in the high-energy state (typhoon or cold winds). When the cobble beach was impacted by high-energy uprush toward the shore and run-up during the typhoon, most cobbles accumulated onshore in the cross-shore direction, and a smaller portion of the cobbles and fine-grained sediments were transported by backwash into the sea. The variation in the profile of the cobble beach was relatively intense, and the cobble beach steepened considerably within a short time. Cobbles accumulated at the location of the beach berm. The height of the beach berm increased, whereas relatively intensive erosion occurred on the

beach face (Alegria-Arzaburu and Masselink, 2010). The height of the beach berm on the cobble beach was closely related to the total run-up elevation during the typhoon process, which was the sum of wave run-up, tidal level, and storm surge (Bergillos *et al*., 2016). The fourth stage was in the restoration state after the typhoon. After the typhoon, the slope of the cobble beach profile became slightly gentler. The width of the beach berm grew, and the height of beach berm declined. During the period of the typhoon, the loss caused by transportation along the coast prevented the profile configuration from returning to the second stage.

5.2 Generation Mechanism of the Erosion Hotspots

Coastal erosion hotspots are defined as the sites where profiles of coasts exhibit significantly higher rates of erosion than adjacent areas (List *et al*., 2006). Erosion hotspots occur on nourished beaches similar to natural beaches (Dean and Dalrymple, 2004). Within three years after the completion of the artificial cobble beach in Tianquan Bay, the retrogression of the coastline was apparent on the west side of the Baishi cape and the west side of the artificial drainpipe rock, and there was also some degree of retrogression of the coastline on the west side of beach near the lower reach of the natural reefs. The cobble beach coastline evolved from being essentially parallel to the artificial revetment upon completion to a slightly curved parabolic shape. Schiaffino *et al*. (2012) adopted the parabola model (Hsu, 1989) to predict the evolution of coastline at 52 beaches along the coast of the Mediterranean, and the results indicated that the modification index of the parabola model can be applied well to gravel beaches (including artificially restored gravel beaches). By comparing the topographic changes of the cobble beach during different stages, three relatively obvious erosion hotspots can be found distributing on the artificial cobble beach from east to west. The main controlling factors for the erosion hotspots of nourishment beaches are coastal underwater topography, sewage pipes, capes, location and direction of the off-shore submerged breakwater, and abrupt change in the trend of the coastline (McNinch, 2004).

When waves propagate from the deep water to nearshore and are blocked by a cape or reef, the waves break because the water depth suddenly becomes shallow. The waves are severely deformed, and energy is concentrated at the front edge of the reef, generating complex nonlinear effects, wave-driven flows, and shallow-water long waves (Chen *et al*., 2000; Kennedy *et al*., 2000; Cavaleri *et al*., 2007). The sea off Tianquan Bay is mainly affected by SE-SSE-trending incident waves and therefore generates a wave-driven coastal current from east to west. Fig.12 shows the distribution of the SSE-trending annual maximum significant wave heights and the wave-driven coastal current in the research area, and the region in the black square is the artificial cobble beach. The Hs in the research area was generally larger than 0.5 m. On the southeast side of the Baishi cape and around the drainpipe and natural reefs, Hs exceeded 1.0 m, and the maximum wave height at the Baishi cape was close to 1.5 m. The figure shows that, relative to the artificial sandy beach on the west side, there is a very obvious large wave height zone near the cobble/sand line of the cobble beach, and Hs is close to 1.0 m. The wave energy strength near the cape, reefs, and drainpipe is stronger than that in other regions. The cobbles constantly accumulate onshore under the action of waves. The slope becomes steeper, and the coastline recedes. Meanwhile, there is a wave-driven coastal current in the direction of WSW to west in the range of the cobble beach, and its maximum flow velocity approaches $1.0\,m\,s^{-1}$, particularly on the two sides of the middle artificial drainpipe. There are small circulations near the Baishi cape, although the coastal current generally flows from east to west with the flow velocity of 0.6 to $1.0\,m\,s^{-1}$. The cobbles are transported from east to west under the action of the wave-driven coastal current. When the transport of cobbles on the profile to the east side is blocked by the drainpipe, they are continuously accumulated on the east side of the drainpipe, whereas cobbles to the west are continuously transported westward without being supplemented. Therefore, the erosion on the profile on the west side of the drainpipe is severe, and the width of the beach berm has declined by more than two-thirds, forming two obvious erosion hotspots on the lower reach side of the coastal current near the coastal headland and the artificial drainpipe. The natural reefs on the west side are relatively far from the shore. Although they cannot directly block the transportation of cobbles, they enhance the coastal current on the lower reach side and cause a small region of erosion hotspots on the shore sitting in the lower reach of the reefs. Fig.13 shows a schematic diagram of the generation mechanism of erosion hotspots in the artificial cobble beach of Tianquan Bay. According to the time scale, the erosion hotspots can be divided into short-term reversible hotspots, medium-term hotspots, and long-term hotspots. Short-term erosion hotspots are reversible and are mainly related to storms, and the durations of medium-term erosion hotspots are a month to a year, which are obviously visible and can be revealed through on-site measurements (Ashton *et al*., 2003; List *et al*., 2006). The erosion hotspot on the artificial cobble beach in Tianquan Bay has been visible for three years and is a medium-term erosion hotspot, which is therefore irreversible. The appearance of an erosion hotspot will affect the stability and re-nourishing cycle of the nourished beach, and we should focus on erosion hotspot regions during beach nourishment.

5.3 Characteristics of Storm Response

The high waves and surges caused by storms are important dynamic factors for the development and evolution of beaches (Elko and Wang, 2007; Grottoli *et al*., 2017). When a storm surge overlaps with high-energy waves, it can cause catastrophic destruction of beach topography and geomorphology within a short time (Ruggiero *et al*., 2001; Pye and Blott, 2008; Masselink *et al*., 2010). This phenomenon is especially apparent on mi-

cro-tidal and mid-tidal beaches and is not completely applicable on macro-tidal beaches. The reason is that the large tidal ranges of macro-tidal beaches limit the time when the heights of the tide plus surge exceed threshold levels and therefore restrict the duration of beach erosion. The duration of the high water level directly affects the intensity of beach erosion (Austin and Buscombe, 2008; Esteves *et al*., 2012). The upper limit height for the action of a storm on a beach is the sum of the astronomical tide level, maximum storm surge and wave run-up, and is affected by many factors such as storm strength, typhoon path, and landing time. Sallenger Jr. (2000) proposed that the storm response model of beaches can be divided into four types: swash, collision, overwash, and inundation. The artificial cobble beach of Tianquan Bay is located on a macro-tidal coast, and Typhoon Meranti landed near the low-tide period of the ebb tide. During the landing of the typhoon and the subsequent impact process, the total level that the astronomical tide and the storm surge added to the wave run-up of the typhoon, which reached a maximum of approximately 4.10 m, is lower than the historical highest water level and the top elevation of the cobble beach berm, without the occurrence of an overwash phenomenon.

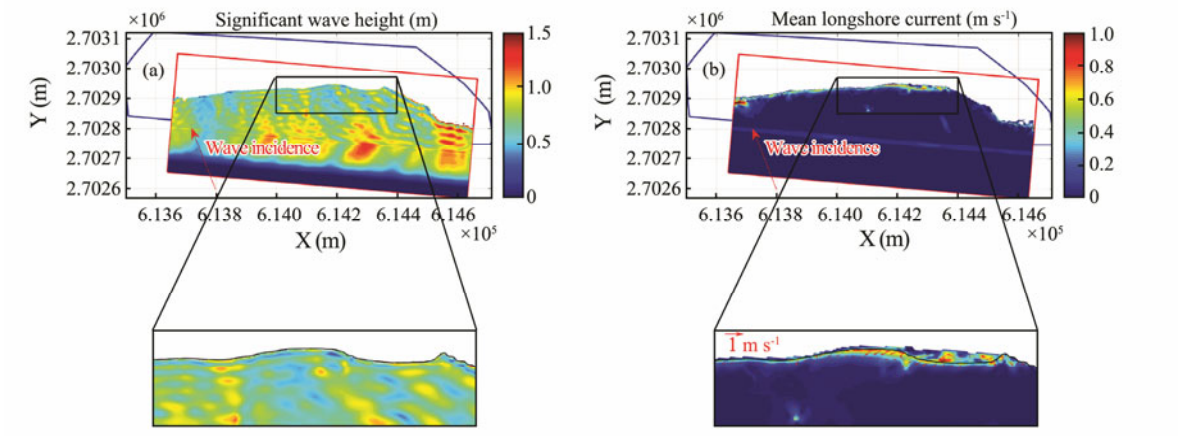

Fig.12 Numerical simulation of the hydrodynamic field on the artificial cobble beach. a, annual maximum Hs; b, wave-driven coastal current.

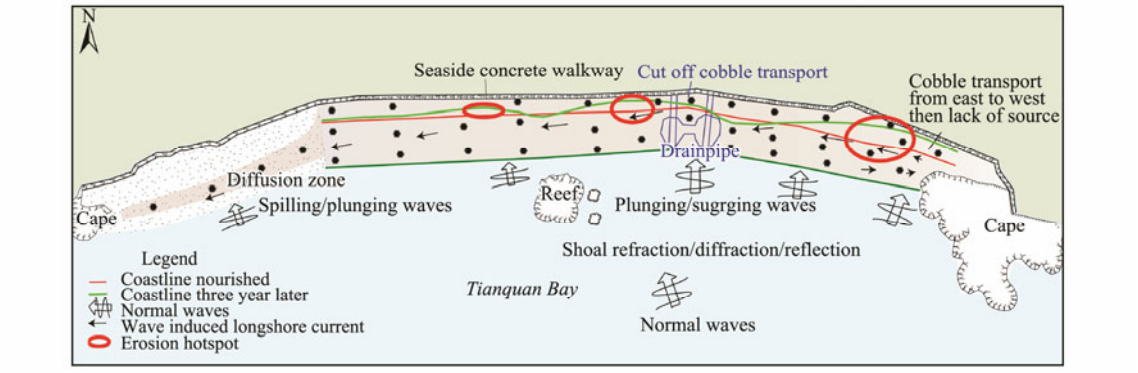

Fig.13 Schematic diagram of the generation mechanism of erosion hotspots on the artificial cobble beach.

Low-tide terrace beaches are generally developed in coastal areas with large tidal ranges (Masselink and Short, 1993), and Xiamen Island has developed the low-tide terrace sandy beaches along the coast. Qi *et al*. (2010) suggested that the response of a low-tide terrace beach to a storm generally exhibits strong erosion on the upper profile and accumulation on the lower profile. The beach berm could be completely eroded in one storm. The action of storms causes strong cross-shore sediment transportation, and the slope of the beach becomes considerably gentler. Before and after Typhoon Meranti, we also monitored the typical profile of the sandy beach near the artificial cobble beach (Fig.1b), and Fig.14 shows a schematic diagram of the storm response for different types of beaches in the research area to Typhoon 'Meranti' (2016 14). What is notably different from the sandy beach is that during the storm, the beach face of the artificial cobble beach was eroded. The majority of cobbles on the beach face are subjected to the effects of uprush caused by high-energy plunging waves, and they are constantly transported onshore, accumulating in the upper part of the beach berm and forming an even higher berm crest. Only a very small portion of cobbles and fine-grained sediments are transported offshore by the backwash, and the slope of the cobble beach becomes considerably steeper. Conversely, the higher beach berm and steeper profile of the cobble beach can dissipate incident high-energy waves more effectively and therefore can protect the coast better. Figs.9c

and 9d also indirectly indicate that after the influence of Typhoon Meranti, the surface of the cobble beach had been eroded, whereas the beach berm had been uplifted because of the accumulation of cobbles, which were the unique response characteristics of the cobble beach to the storm.

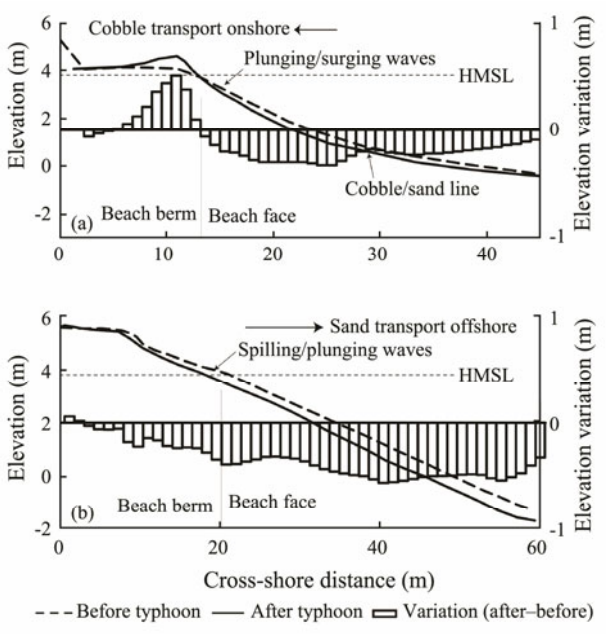

Fig.14 Storm response characteristics of beaches. a, artificial cobble beach, profile P4 in Tianquan bay; b, sandy beach, profile P23 in Taiyang bay.

In the longshore direction, there was apparent transport of cobbles from east to west on the cobble beach after the typhoon, and the cobble diffusion zone also continued to extend to the west. In the process of the typhoon, the total volume of the beach decreased by $4.5\times10^3\,m^3$ (including longshore and offshore losses), and the amount of loss accounted for 11% of the restoration amount on the cobble beach, reaching 50% of the total loss amount on this beach within three years. Alegria-Arzaburu and Masselink (2010) also found that storms (swell waves) can result in the accretion of the supratidal zone and the erosion of the intertidal zone, and a significant loss in overall beach volume. Presuming that sediments for beach nourishment are sands with particle sizes of 0.5 mm, the CERC formula (US Army Corps of Engineers, 2002) and the Kamphuis formula (Kamphuis, 1991) were used to estimate the amount of longshore sediment transport. During typhoons it exceeds $15.0\times10^3\,m^3$, which is much larger than the actual amount lost from the artificial cobble beach. This result also demonstrates that under strong dynamic conditions, cobbles are more stable than sands and can protect the coast better from severe erosion.

6 Conclusions

In this paper, by analyzing the profile configurations and topographic characteristics of a cobble beach during different periods, we obtained the following conclusions.

1) The artificial cobble beach in Tianquan Bay is located on a macro-tidal coast, and it is subject to the action of SE-SSE-trending waves in open seas. After the completion of the artificial cobble beach, the evolution of its profile configuration can be divided into four stages. The beach was unstable during the initial stage after nourishment. There was an obvious change in the profile configuration at this stage and an obvious upper concave composite cobble beach that was steep in the upper part and gentle in the lower part was formed. During the second stage, the cobble beach approached dynamic equilibrium, and the change in the profile configuration was very small. The third stage the beach was in a high-energy state under the influence of a typhoon, and the profile of the cobble beach steepened considerably in a short time. The beach face underwent severe erosion, and the significant accretion occurred at the location of the beach berm. The height of beach berm increased, and the total volume of the beach decreased. The fourth stage was the restoration stage after the typhoon. The slope of the cobble beach became gentler, the width of the beach berm increased, and the height of the beach berm declined.

2) Because of the actions of waves and the wave-driven coastal current under the specific topographic and geomorphological conditions (coastal headland, drainpipe rock, and natural reefs), the coastline of the artificial cobble beach gradually evolved from being essentially parallel to the artificial coast upon completion to a slightly curved parabolic shape, and three obvious erosion hotspots were formed. These erosion hotspots tend to be distributed on the lower reach side of the coastal current in the vicinities of the cape, drainpipe, and reefs.

3) When Typhoon Meranti landed in Xiamen, it was near the low-tide period of the ebb tide, and the cobble beach did not exhibit an overwash phenomenon. The response of the artificial cobble beach to the storm was completely different from the response characteristics of the low-tide terrace sandy beach. There was net transport of cobbles onshore in the cross-shore direction, the beach face was eroded, and the beach berm was uplifted because of accumulation of cobbles. The height of the beach berm increased, and the slope of the profile became steeper. In the longshore direction, the cobble beach experienced considerable transport of cobbles from east to west, and the total volume of the beach during the typhoon process decreased by $4.5\times10^3\,m^3$ (including longshore and offshore losses). The amount accounted for 11% of the restored amount on the cobble beach and reached 50% of the total amount lost from the beach over three years.

Acknowledgements

This research was supported by the Scientific Research Foundation of the Third Institute of Oceanography, State Oceanic Administration (Nos. 20170305, 2011010) and the Public Science and Technology Research Funds Projects of Ocean (No. 201405037). We thank all of the investigators for their help in collecting data during the ob-

servations. Special thanks go to Drs. Yue Yu, Gen Liu and Yang Lu for their field efforts. We are thankful to the anonymous reviewers whose valuable comments helped improve the original manuscript.

References

Alegria-Arzaburu, A. R. D., and Masselink, G., 2010. Storm response and beach rotation on a gravel beach, Slapton Sands, U. K. *Marine Geology*, **278** (1-4): 77-99.

Aminti, P., Cipriani, L. E., and Pranzini, E., 2003. *'Back to the Beach': Converting Seawalls into Gravel Beaches*. Springer, Dordrecht, Netherlands, 261-274.

Anthony, E. J., 2005. *Beach Erosion*. *Encyclopedia of Coastal Science*. Springer, Dordrecht, Netherlands, 140-145.

Aragonés, L., Garcia-Barba, J., García-Bleda, E., Lopez, I., and Serra, J. C., 2015. Beach nourishment impact on *Posidonia oceanica*: Case study of Poniente Beach (Benidorm, Spain). *Ocean Engineering*, **107** (7): 1-12.

Ashton, A., List, J. H., Murray, A. B., and Farris, A. S., 2003. Links between erosional hotspots and alongshore sediment transport. *Coastal Sediments' 03, Annual Symposium on Coastal Engineering and Science of Coastal Sediment Processes*, 1-13.

Austin, M. J., and Buscombe, D., 2008. Morphological change and sediment dynamics of the beach step on a macrotidal gravel beach. *Marine Geology*, **249** (3-4): 167-183.

Austin, M. J., and Masselink, G., 2005. Infiltration and exfiltration on a steep gravel beach: Implications for sediment transport. *Coastal Dynamics 2005: State of the Practice*. Barcelone, 1-14.

Austin, M. J., and Masselink, G., 2006. Observations of morphological change and sediment transport on a steep gravel beach. *Marine Geology*, **229** (1-2): 59-77.

Bergillos, R. J., Rodríguez-Delgado, C., and Ortega-Sánchez, M., 2017. Advances in management tools for modeling artificial nourishments in mixed beaches. *Journal of Marine Systems*, **172**: 1-13.

Bergillos, R. J., Ortega-Sánchez, M., and Losada, M. A., 2015. Foreshore evolution of a mixed sand and gravel beach: The case of Playa Granada (southern Spain). *The Proceedings of the Coastal Sediments*, San Diego, USA, 1-14.

Bergillos, R. J., Ortega-Sánchez, M., Masselink, G., and Losada, M. A., 2016. Morpho-sedimentary dynamics of a micro-tidal mixed sand and gravel beach, Playa Granada, southern Spain. *Marine Geology*, **379**: 28-38.

Bertoni, D., and Sarti, G., 2011. On the profile evolution of three artificial pebble beaches at Marina di Pisa, Italy. *Geomorphology*, **130** (3-4): 244-254.

Bird, E. C. F., 1985. *Coastline Changes: A Global Review*. John Wiley and Sons Inc., New York, 1-231.

Bruun, P., 1988. The Bruun rule of erosion by sea-level rise: A discussion on large-scale two- and three-dimensional usages. *Journal of Coastal Research*, **4** (4): 627-648.

Cai, F., Dean, R. G., and Liu, J., 2011. Beach nourishment in China: Status and prospects. *Coastal Engineering Proceedings*, **1** (32): 31.

Cai, F., Su, X., Liu, J., Li, B., and Lei, G., 2009. Coastal erosion in China under the condition of global climate change and measures for its prevention. *Progress in Natural Science*, **19** (4): 415-426.

Cammelli, C., Jackson, N. L., Nordstrom, K. F., and Pranzini, E., 2006. Assessment of a gravel nourishment project fronting a seawall at Marina di Pisa, Italy. *Journal of Coastal Research*, **39** (39): 770-775.

Castelle, B., Marieu, V., Bujan, S., Splinter, K. D., Robinet, A., Sénéchal, N., and Ferreira, S., 2015. Impact of the winter 2013–2014 series of severe Western Europe storms on a double-barred sandy coast: Beach and dune erosion and megacusp embayments. *Geomorphology*, **238**: 135-148.

Cavaleri, L., Alves, J. H., Ardhuin, F., Babanin, A., Banner, M., Belibassakis, K., and Hwang, P. A. E. M., 2007. Wave modelling – The state of the art. *Progress in Oceanography*, **75** (4): 603-674.

Chen, B., and Stephenson, W., 2015. Measuring pebble abrasion on a mixed sand and gravel beach using abrasion baskets. *Geomorphology*, **248**: 24-32.

Chen, B., Chen, Z., Stephenson, W., and Finlayson, B., 2011. Morphodynamics of a boulder beach, Putuo Island, SE China coast: The role of storms and typhoon. *Marine Geology*, **283** (1-4): 106-115.

Chen, Q., Kirby, J. T., Dalrymple, R. A., Kennedy, A. B., and Chawla, A., 2000. Boussinesq modeling of wave transformation, breaking, and runup. II: 2D. *Journal of Waterway, Port, Coastal, and Ocean Engineering*, **126** (1): 48-56.

Davison, A. T., Nicholls, R. J., and Leatherman, S. P., 1992. Beach nourishment as a coastal management tool: An annotated bibliography on developments associated with the artificial nourishment of beaches. *Journal of Coastal Research*, **8** (4): 984-1022.

Dean, R. G., 2005. Beach nourishment: Benefits, theory and case examples. In: *Environmentally Friendly Coastal Protection*. Springer, Dordrecht, 25-40.

Dean, R. G., and Dalrymple, R. A., 2004. *Coastal Processes with Engineering Applications*. Cambridge University Press, Cambridge, 1-487.

Dixon, K. L., and Pilkey Jr., O. H., 1991. Summary of beach replenishment on the U. S. Gulf of Mexico shoreline. *Journal of Coastal Research*, **7** (1): 249-256.

Elko, N. A., and Wang, P., 2007. Immediate profile and planform evolution of a beach nourishment project with hurricane influences. *Coastal Engineering*, **54** (1): 49-66.

Esteves, L. S., Brown, J. M., Williams, J. J., and Lymbery, G., 2012. Quantifying thresholds for significant dune erosion along the Sefton Coast, Northwest England. *Geomorphology*, **143**: 52-61.

Fu, X., Wu, S., Li, T., Hou, J., and Liu, Q., 2013. Characteristics analysis of tide along Fujian mid-south coastal waters. *Journal of Applied Oceanography*, **32** (2): 164-170.

Gorzelany, J. F., and Nelson, W. G., 1987. The effects of beach replenishment on the benthos of a sub-tropical Florida beach. *Marine Environmental Research*, **21** (2): 75-94.

Grottoli, E., Bertoni, D., and Ciavola, P., 2017. Short- and medium-term response to storms on three mediterranean coarse-grained beaches. *Geomorphology*, **295**: 738-748.

Haerens, P., Bolle, A., Trouw, K., and Houthuys, R., 2012. Definition of storm thresholds for significant morphological change of the sandy beaches along the Belgian coastline. *Geomorphology*, **143**: 104-117.

Hanson, H., Brampton, A., Capobianco, M., Dette, H. H., Hamm, L., Laustrup, C., and Spanhoff, R., 2002. Beach nourishment projects, practices, and objectives – A European overview. *Coastal Engineering*, **47** (2): 81-111.

Ha, T., Jun, K., Yoo, J., and Park, K. S., 2014. Numerical study of rip current generation mechanism at Haeundae Beach, Korea. *Journal of Coastal Research*, **72** (sp1): 179-183.

Hine, A. C., 1979. Mechanisms of berm development and re-

sulting beach growth along a barrier spit complex. *Sedimentology*, **26** (3): 333-351.

Hsu, J. R. C., 1989. Parabolic bay shapes and applications. *Proceedings of the Institution of Civil Engineers*, **87**: 557-570.

Kamphuis, J. W., 1991. Alongshore sediment transport rate. *Journal of Waterway, Port, Coastal, and Ocean Engineering*. **117** (6): 624-640.

Kennedy, A. B., Chen, Q., Kirby, J. T., and Dalrymple, R. A., 2000. Boussinesq modeling of wave transformation, breaking, and runup. I: 1D. *Journal of Waterway, Port, Coastal, and Ocean Engineering*, **126** (1): 39-47.

Kirby, J. T., Wei, G., Chen, Q., Kennedy, A. B., and Dalrymple, R. A., 1998. Funwave 1.0. Fully nonlinear boussinesq wave model. Documentation and User's Manual. University of Delaware.

Kirk, R. M., 1992. Artificial beach growth for breakwater protection at the Port of Timaru, east coast, South Island, New Zealand. *Coastal Engineering*, **17** (3-4): 227-251.

Liao, K., Wang, Y., He, J., Lin, Y., and Chen, Z., 2010. Research report on tidal characteristics in Fujian coast. Third Institute of Oceanography, State Oceanic Administration, Xiamen, 1-54.

List, J. H., Farris, A. S., and Sullivan, C., 2006. Reversing storm hotspots on sandy beaches: Spatial and temporal characteristics. *Marine Geology*, **226** (3-4): 261-279.

López, I., Aragonés, L., Villacampa, Y., Compañ, P., and Satorre, R., 2015. Morphological classification of microtidal sand and gravel beaches. *Ocean Engineering*, **109**: 309-319.

Lorang, M. S., 1991. An artificial perched-gravel beach as a shore protection structure. *Proceedings of Coastal Sediments '91 American Society of Civil Engineers*. New York, 1916-1925.

Masselink, G., and Short, A. D., 1993. The effect of tide range on beach morphodynamics and morphology: A conceptual beach model. *Journal of Coastal Research*, **9** (3): 785-800.

Masselink, G., Russell, P., Blenkinsopp, C., and Turner, I., 2010. Swash zone sediment transport, step dynamics and morphological response on a gravel beach. *Marine Geology*, **274** (1-4): 50-68.

Masselink, G., Scott, T., Poate, T., Russell, P., Davidson, M., and Conley, D., 2016. The extreme 2013/2014 winter storms: Hydrodynamic forcing and coastal response along the southwest coast of England. *Earth Surface Processes and Landforms*, **41** (3): 378-391.

McNinch, J. E., 2004. Geologic control in the nearshore: Shore-oblique sandbars and shoreline erosional hotspots, Mid-Atlantic Bight, USA. *Marine Geology*, **211** (1-2): 121-141.

Neumann, B., Vafeidis, A. T., Zimmermann, J., and Nicholls, R. J., 2015. Future coastal population growth and exposure to sea-level rise and coastal flooding-a global assessment. *PLoS One*, **10** (3): e0118571.

Osborne, P. D., 2005. Transport of gravel and cobble on a mixed-sediment inner bank shoreline of a large inlet, Grays Harbor, Washington. *Marine Geology*, **224** (1-4): 145-156.

Pedrozo-Acuña, A., Simmonds, D. J., Chadwick, A. J., and Silva, R., 2007. A numerical-empirical approach for evaluating morphodynamic processes on gravel and mixed sand-gravel beaches. *Marine Geology*, **241** (1-4): 1-18.

Pedrozo-Acuña, A., Simmonds, D. J., and Reeve, D. E., 2008. Wave-impact characteristics of plunging breakers acting on gravel beaches. *Marine Geology*, **253** (1-2): 26-35.

Pilkey, O. H., 1990. A time to look back at beach replenishment. *Journal of Coastal Research*, **6** (1): iii-vii.

Pilkey Jr., O. H., and Cooper, J. A. G., 2014. *The Last Beach*. Duke University Press, Durham, 1-233.

Pye, K., and Blott, S. J., 2008. Decadal-scale variation in dune erosion and accretion rates: An investigation of the significance of changing storm tide frequency and magnitude on the Sefton coast, UK. *Geomorphology*, **102** (3-4): 652-666.

Pye, K., and Blott, S. J., 2009. Progressive breakdown of a gravel-dominated coastal barrier, Dunwich-Walberswick, Suffolk, U. K.: Processes and implications. *Journal of Coastal Research*, **25** (3): 589-602.

Qi, H., Cai, F., Lei, G., Cao, H., and Shi, F., 2010. The response of three main beach types to tropical storms in South China. *Marine Geology*, **275** (1-4): 244-254.

Ruggiero, P., Komar, P. D., McDougal, W. G., Marra, J. J., and Beach, R. A., 2001. Wave runup, extreme water levels and the erosion of properties backing beaches. *Journal of Coastal Research*, **17** (2): 407-419.

Sallenger Jr., A. H., 2000. Storm impact scale for barrier islands. *Journal of Coastal Research*, **16** (3): 890-895.

Schiaffino, C. F., Brignone, M., and Ferrari, M., 2012. Application of the parabolic bay shape equation to sand and gravel beaches on Mediterranean coasts. *Coastal Engineering*, **59** (1): 57-63.

Shi, F., Kirby, J. T., Harris, J. C., Geiman, J. D., and Grilli, S. T., 2012. A high-order adaptive time-stepping TVD solver for Boussinesq modeling of breaking waves and coastal inundation. *Ocean Modelling*, **43**: 36-51.

Shi, F., Tehranirad, B., James, T. K., Harris, J. C., and Grilli, S., 2013. Funwave-TVD fully nonlinear boussinesq wave model with TVD solver documentation and user's manual (Version 2.1). http://www1.udel.edu/kirby/papers/shi-etal-cacr-11-04-version2.1.pdf.

Stark, N., and Hay, A. E., 2016. Pebble and cobble transport on a steep, mega-tidal, mixed sand and gravel beach. *Marine Geology*, **382**: 210-223.

Su, S. F., Ma, G., and Hsu, T. W., 2015. Boussinesq modeling of spatial variability of infragravity waves on fringing reefs. *Ocean Engineering*, **101**: 78-92.

US Army Corps of Engineers, 2002. Coastal engineering manual. Department of the Army, US Army Corpos of Engineers, **III** (2): 10-15.

Van Rijn, L. C., 2011. Coastal erosion and control. *Ocean & Coastal Management*, **54** (12): 867-887.

Zenkovich, V. P., and Schwartz, M. L., 1987. Protecting the Black Sea–Georgian S. S. R. gravel coast. *Journal of Coastal Research*, **3** (2): 201-209.

(Edited by Chen Wenwen)